International Journal of Mechanical Sciences 206 (2021) 106621

Contents lists available at ScienceDirect

International Journal of Mechanical Sciences

journal homepage: www.elsevier.com/locate/ijmecsci

Finite element analysis of a self-propelled capsule robot moving in the small intestine

Jiyuan Tian[a], Yang Liu[a,*], Junning Chen[a], Bingyong Guo[a], Shyam Prasad[b]

[a] College of Engineering, Mathematics and Physical Sciences, University of Exeter, North Park Road, Exeter, EX4 4QF, UK
[b] The Royal Devon and Exeter NHS Foundation Trust, Barrack Road, Exeter, EX2 5DW, UK

ARTICLE INFO

Keywords:
Capsule endoscopy
Small intestine
Finite element
Capsule robot
Contact pressure

ABSTRACT

In order to optimise the passage of the self-propelled capsule robot in the small intestine, capsule-intestine interactions were studied in this paper via finite element (FE) analysis and experimental investigation. Different contact conditions were considered to reflect the structural complexity and motility of the intestinal tract, including the flat-open, collapsed, contractive and curved intestines. Capsule's geometric shape and progression speed are the two major factors to be optimised against the intestinal trauma caused by capsule-intestine contact and friction. In addition, the mesentery was also considered as the intestinal boundary to restrict the mobility of the intestine. By comparing with the experimental results, the proposed FE model can provide quantitative estimations of contact pressure and resistance force under different capsule-intestine conditions. The findings of this work are valuable to provide design guidelines and an evaluation means for the researchers and engineers who are developing medical robots for bowel examination as well as the clinical practitioners working in capsule endoscopy.

1. Introduction

Swallowable capsule endoscope offers patients a non-invasive and comfortable modality when detecting the gastrointestinal (GI) diseases effectively [1,2], such as polyposis syndrome, coeliac disease, ulcerative colitis and obscure bleeding [2–4], over the conventional lower GI endoscopy. Although several capsule endoscopes [5–7] have been commercialised in the last two decades, there are still some critical challenges that remain open, e.g. the inability of obtaining biopsy specimens and implementing therapeutic procedures [8], and lack of motion control [9]. At the moment, all the commercialised capsule endoscopes for small-bowel examination are passively driven by the intestinal peristalsis [10]. However, this passive locomotion could lead to significant limitations, in particular due to the unpredictable and variable transit speeds [11]. Significant abnormalities, e.g. small-bowel bleeding, may be missed and lead to incomplete visualisation of the intestinal surface. Therefore, the current procedure is considered both time-consuming and burdensome for clinicians and patients.

Controlling capsule's passage in the small bowel is a challenging but essential task. There are four factors that affect capsule's motility, including the complex anatomy of the intestine, dynamic peristaltic patterns, various contact conditions between the capsule and the intestinal lumen, and nonlinear behaviour of the intestinal mucosa. After swallowing, the capsule will go through the oesophagus, stomach, small intestine and colon before being excreted from the anus [10]. Compared to the other organs, the small intestine has a more complicated anatomy. A typical cross-section of the small-bowel wall is presented in Fig. 1(a) which includes a connective tissue layer (the serosa), a longitudinal muscle layer, a circular muscle layer, the submucosa and the mucosa [12]. The mesentery connected to the serosa is not always presented in the small intestine depending on the age group of the patients, so the abdominal cavity can be considered as either mesenteric or non–mesenteric [13]. Since the mesentery could restrict the mobility of the intestine, this may lead to different capsule-intestine contact conditions. Therefore, a comparative study of capsule's passage in both mesenteric and non–mesenteric intestines is needed. On the other hand, in the perspective of cellular scale, there is a layer of epithelial cell lined on the outermost layer of the mucosa, contacting with the intestinal lumen. These epithelial cells that fold into the villus and adjacent crypts as shown in Fig. 1(b) are used to digest nutrients from the chyme and deliver them to the blood vessels in the submucosa to provide human needs [14]. The location of the crypt is the most commonplace for polyp and tumour initiations [15], which requires to use a diagnostic tool to examine carefully at an early stage. Thus the detection accuracy of the nidus location by using capsule endoscopy can be affected significantly by the complexity of small-bowel anatomy, especially for the early-stage

* Corresponding author.
E-mail addresses: jt535@exeter.ac.uk (J. Tian), y.liu2@exeter.ac.uk (Y. Liu), J.Chen3@exeter.ac.uk (J. Chen), b.guo@exeter.ac.uk (B. Guo), shyamprasad@nhs.net (S. Prasad).

https://doi.org/10.1016/j.ijmecsci.2021.106621
Received 24 March 2021; Received in revised form 11 June 2021; Accepted 23 June 2021
Available online 24 June 2021

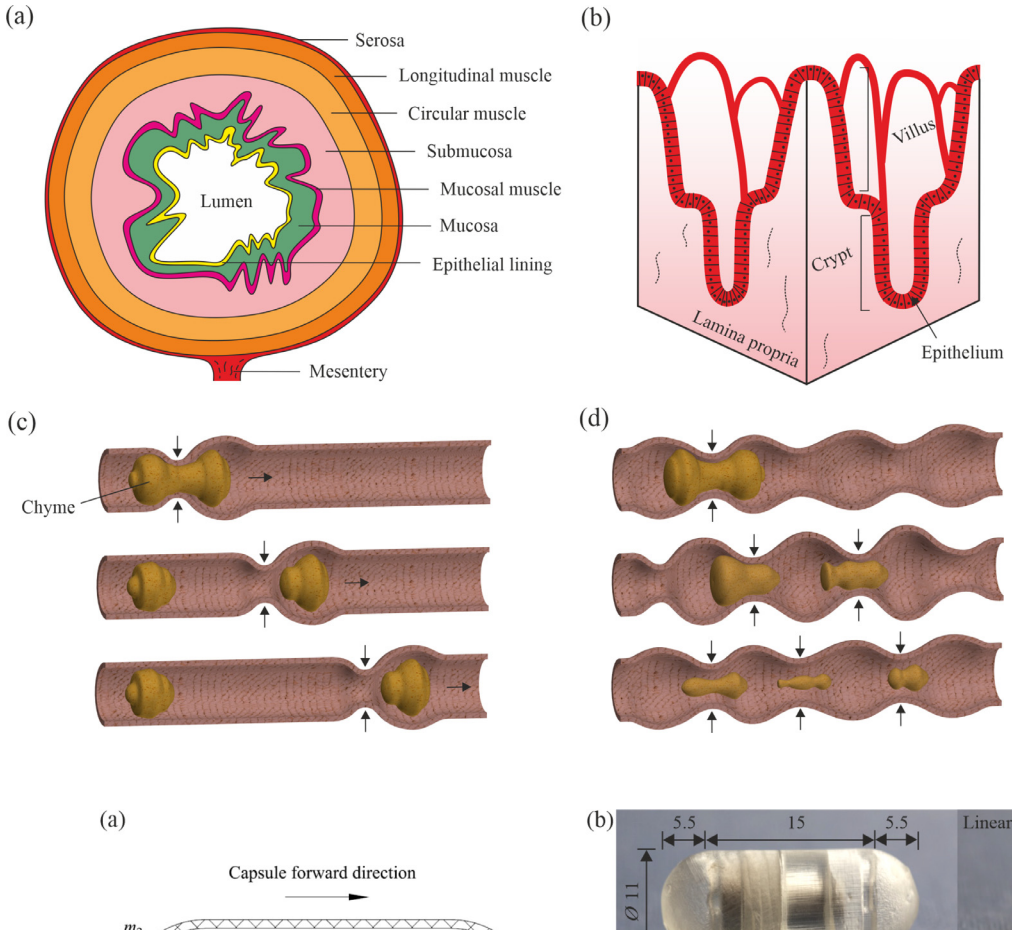

Fig. 1. (Colour online) (a) Cross-section of the intestinal wall. (b) Structure of the intestinal villi and crypt. (c) Peristalsis of the small intestine. (e) Segmentation of the small intestine.

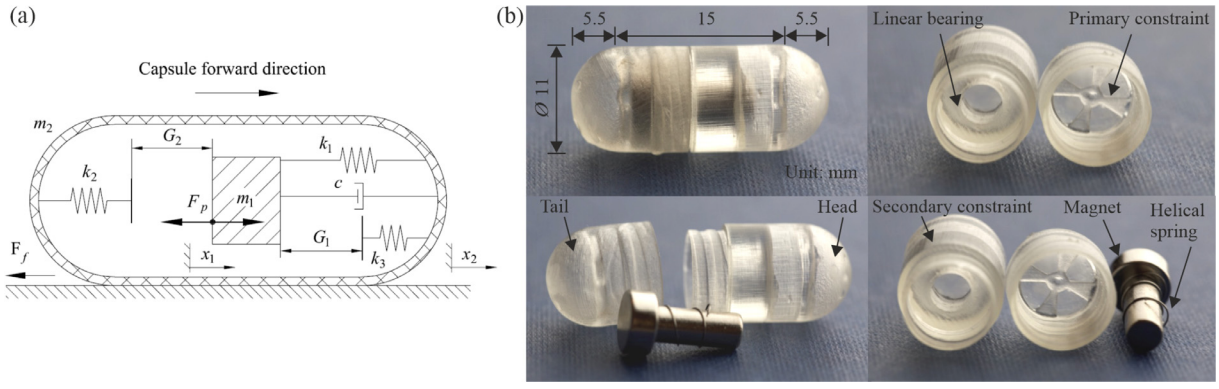

Fig. 2. (a) Physical model and (b) prototype design of the vibro-impact capsule system developed by Liu et al. [22].

lesions. In addition, the dynamic motile patterns of the intestinal tract also induce uncertainties on capsule's locomotion. In general, peristalsis and segmentation presented in Figs. 1(c) and (d) are the two basic movements of the small intestine, including propulsive and mixing contractions [12,14]. Peristalsis is formed by the successive motions of the contraction and the expansion ring, while segmentation is performed by the alternate contraction ring along the small intestine. These two motions together with the twisted and interwoven arrangement of the intestine make the pressure and resistance force between the capsule and the intestine more difficult to be predicted. Therefore studying different capsule-intestine interactions is essential for the motion control of capsule endoscopy.

Intestinal modelling was studied in terms of the hyperelastic [16,17] and viscoelastic [18–20] properties of the intestine. Ciarletta et al. [16] studied the stress-strain relationship of the intestinal longitudinal muscle layer and the circumferential muscle layer by using a hyperelastic constitutive model. Zhang and Liu [21] subsequently found that the mucosal and the epithelial layers are viscoelastic, while the hyperelasticity mainly comes from the muscle layer. However, viscoelasticity was commonly used to represent the characteristics of the intestinal material, since it can better describe the time-dependent mechanical characteristics of the intestinal tissue. Therefore, in the present paper, we will study the contact pressure between the moving capsule and the intestine by considering the viscoelasticity of the intestine under different capsule-intestine interactions.

In order to control capsule's motion in the intestine, some driving mechanisms have been developed, such as the paddle-type capsule [23], the legged capsule [24], the inchworm-like capsule [25], the propeller-based capsule [26], the vibration capsule [27,28] and the spiral-based capsule [19]. However, most of these locomotion solutions require external accessories outside of the capsule, such as arms, fins or propellers, all of which could cause intestinal trauma. Therefore, the active capsule

with an original smooth surface is more user-friendly and clinically acceptable. Chernousko [29] has proposed that the rectilinear motion of a system can be obtained by controlling the interaction between two rigid bodies in the presence of environmental resistance. A similar driving principle has been widely adopted in vibro-impact drilling [30], capsule endoscopy [31], and pipeline inspection [32]. Liu et al. [27,33] carried out a fundamental study on a vibro-impact capsule system shown in Fig. 2(a), which is self-propelled without any external moving parts. It can be seen from the figure that the system consists of a smooth rigid shell (m_2) connected with an internal mass (m_1) via a helical spring (k_1) and a viscous damper (c). The internal mass driven by a periodic force (F_p) collides with the primary (k_2) and the secondary constraints (k_3) once the relative displacement between the capsule and the internal mass is larger or equal to the gaps, G_1 and G_2, respectively. When the net force on the capsule exceeds the intestinal resistance (F_f), the entire capsule will move forward or backward in the intestine. For the equations of motion of the capsule system, readers can refer to Appendix. The dynamic characteristics of the capsule were further developed in terms of the capsule progression speed and energy efficiency under various control parameters and frictional environments, see e.g. [34–38]. Fig. 2(b) presents the prototype of the capsule system in millimetre scale, where a T-shape magnet excited by an external magnetic field was considered as the internal mass, and two structural springs with the same geometric design were adopted as the primary and secondary constraints. Since the magnet has two different diameters for the front and the end cross-sections, this can lead to two different stiffness (k_2 and k_3) when the magnet impacts with the structural springs. In this work, we will present both numerical study and experimental investigation by using this capsule prototype.

Commercialised capsule endoscopes and newly developed active capsules always have a cylindrical body with a semi-circled head and tail, but the optimisation studies about their shapes from the literature are very rare. In particular, the capsule experiences various capsule-intestine interactions due to the peristalsis of the small intestine. A comprehensive model of the capsule-intestine interaction that can predict their contact pressure, frictional resistance and capsule's progression speed is essential. This is particularly important for the real scenario when the small intestine naturally gets twisted with varying radii in the patient's abdominal cavity. Furthermore, capsule's locomotion in the mesenteric small intestine was also rarely studied. Relevant research works focused on investigating the influence of capsule's shape [39], dimension [18], weight [40], material and moving speed [19,41–47] on the intestinal resistance. However, these studies were only based on a simple capsule-intestine contact model without considering the intestinal anatomy. For the self-propulsion of the vibro-impact capsule [22] in the small intestine, the effect of vibrational motion of the capsule on the intestine in terms of its contact pressure and intestinal resistance has not been fully studied yet. Previous studies mainly concentrated on mathematical modelling [36] and experimental verification [20], and only few studies considered the simplified capsule-intestine model by using finite element (FE) analysis, e.g. [40]. These unsolved issues are the motivation of our research work presented in this paper.

The aim of this paper is to study the interaction between the moving capsule and the small intestine through FE analysis and experimental investigation, which can be used to guide the control design of the vibro-impact capsule system [27]. Compared to our previous study [20], the contributions of the present work were summarized as follow. (i) Both constant and varying speeds of the capsule moving in the small intestine were considered in this study. (ii) The intestine with and without mesentery were investigated. (iii) The curved intestines with different bending radii were considered. (iv) Capsule's shape and the intestinal trauma in terms of capsule-intestine contact pressure were studied. (v) The influence of the vibro-impact motion on the intestine caused by the vibrational capsule was also investigated.

The rest of this paper is organised as follows. In Section 2, FE modelling of the capsule-intestine interaction was firstly studied for capsule's shape optimisation. The potential intestinal trauma caused by different capsule's shapes and dimensions were evaluated according to [48]. Four different contact cases, including the capsule moving through a flat-open, a collapsed, a contractive or a curved intestine at various speeds, were considered for evaluating the contact pressure and the intestinal resistance between the capsule and the small intestine. In addition, the FE results of the curved intestine with and without the mesentery were also compared. In Section 3, the experimental setup for measuring the contact pressure under various capsule's speeds and the experimental rig of the vibro-impact capsule system were introduced. Section 4 presents the speed-dependent analysis by using the FE model in comparison with experimental results. In Section 5, the influence of the bending radius of the intestine on capsule-intestine contact with and without the mesentery is studied. To understand the influence of the capsule's shape, various shapes of the capsule are studied in Section 6. Then in Section 7, the capsule' progression obtained from the experimental rig was adopted in the FE model to evaluate the contact pressure caused by the vibro-impact mechanism. Finally, conclusions and future works are drawn in Section 8.

2. Finite element modelling of the capsule-intestine contact

In the present work, numerical analysis using FE method was conducted using ANSYS WORKBENCH 19.0/transient structural model, in which an implicit dynamic solver was applied. In order to take into account the peristalsis of the small intestine (at a rate of 8-11 cycles per minute) and the complex intestinal anatomy, four contact cases mimicking the real capsule-intestine contact scenarios were implemented as illustrated in Fig. 3, including the capsule moving in a flat-open, a naturally collapsed, a contractive and a curved intestines.

2.1. Model description and material properties

For Case 1, when the small intestine expands, the upper intestinal wall is far away from the capsule and only the lower wall is in contact with the capsule as presented in Fig. 3(a). In this case, the contact pressure between the capsule and the lower intestinal wall only relies on capsule's gravity which can be calculated analytically by using the Hertz contact theory [20]. As the intestine relaxes, the upper wall of the intestine falls naturally on the moving capsule in Case 2 due to gravity as shown in Fig. 3(b). In this scenario, the capsule-intestine contact pressure is subject to the gravity of the capsule and the upper section of the intestine, and their contact areas include both the upper and the lower surfaces of the capsule. Due to the intestinal peristalsis, the intestine may produce a certain length of contractive ring. For Case 3 as presented in Fig. 3(c), since the diameter of the capsule is larger than the diameter of the contractive intestine, the capsule is subject to intestinal hoop pressure, and the detailed modelling of the hoop pressure can be found in [20]. Case 4 shown in Fig. 3(d) simulates the capsule moving in a curved intestine. In this condition, the hoop stress acting on the capsule is not circumferentially symmetric anymore, and the tangential stress changes along the circumference of the small intestine.

The viscoelastic properties of the synthetic small intestine used in this work were studied in [20]. A three-element Maxwell model consisting of two elastic springs and a viscous damper written as

$$E(t) = E_1 e^{-\frac{E_1}{\eta_1}t} + E_2, \tag{1}$$

was employed to represent the stress-strain relationship of the small intestine, where E_1 and E_2 are the Young's moduli of the springs, η_1 is the viscosity coefficient of the damper. The hoop stress of the intestine can be calculated as

$$\sigma = \epsilon E(t), \tag{2}$$

where $\epsilon = (R_i - R_c)/R_i$ is the intestinal strain, R_c is the external radius of the capsule and R_i is the internal radius of the intestine. Since the small intestine used in this study was synthesized from human tissue

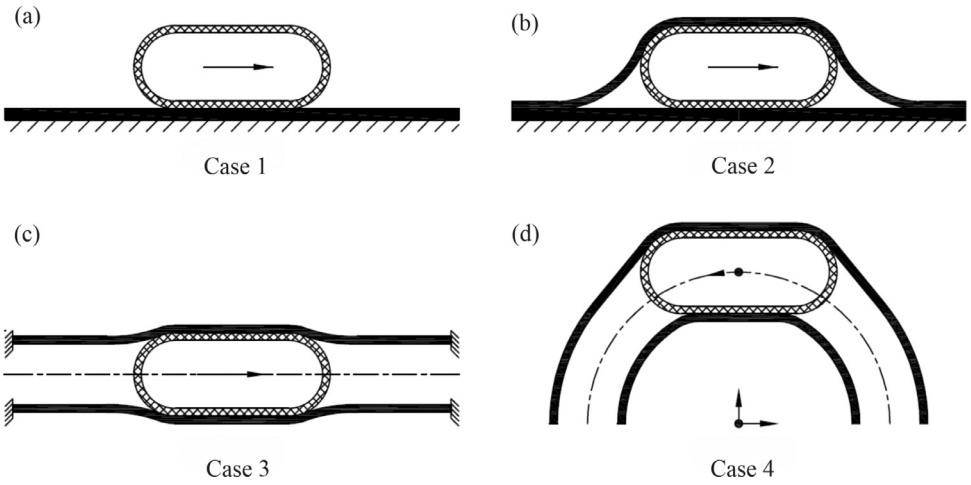

Fig. 3. Schematic diagrams of the capsule moving in (a) Case 1: flat-open intestine, (b) Case 2: collapsed intestine, (c) Case 3: contractive intestine, (d) Case 4: curved intestine.

Table 1
Material parameters of the capsule and the synthetic small intestine.

Material Parameters	Value	Unit
E_c	0.11	GPa
ν_c	0.42	-
ρ_c	0.95	g/mm^3
E_t	25	kPa
E_f	953.91	kPa
E_1	196.43	kPa
E_2	757.48	kPa
η_1	5.36	MPa·s
ν_i	0.49	-
ρ_i	1	g/mm^3
μ	0.2293	-

analogues and woven fibres, its mechanical properties are dominant by the tissue analogues with Young's modulus E_t provided by the manufacturer [49] when the intestine is compressed. When the intestine is expanded by the capsule, the woven fibres with Young's modulus E_f dominate its mechanical properties. Therefore, in our FE simulations, E_t was used for Case 1 and 2, and E_f that was identified through our stress relaxation tests [20] was adopted for Case 3 and 4. All the parameters of the polyethene capsule and the synthetic small intestine are presented in Table 1, where E_c is the Young's modulus of the capsule, ν_c is Poisson's ratio of the capsule, ρ_c is the density of the capsule, ν_i is the Poisson's ratio of the intestine, ρ_i is the density of the intestine and μ is the friction coefficient between the capsule and the small intestine.

2.2. Model configurations

The capsule adopted in this study is 11 mm in diameter, 26 mm in length, 0.5 mm for its shell's thickness, and 3.47 g for the total weight, which were obtained from the prototype shown in Fig. 2(b). For Cases 1 to 4, the thickness of the small intestine was all set at 0.69 mm which was consistent with our experiment. In order to build the FE model, some geometric and material assumptions are introduced as follows.

- The thickness of the original intestinal wall was assumed uniform along the intestine, which has the same dimension as the synthetic small intestine used in our experiment.
- For Cases 3 and 4, the intestinal wall was assumed to be a straight and a curved circular tubes with their inner diameters smaller than the outer diameter of the capsule.
- Because of symmetry, only one quarter of the model of Case 3 was computed in order to reduce the computational cost.
- The small intestine is isotropic, homogeneous and nearly incompressible.

Case 1 considers a capsule moving on a cut-open intestine supported by a fixed steel plate as shown in Fig. 4(a). For the requirement of deformation, two types of elements were used to mesh the model. The 8-node solid element (SOLID185) was used for the capsule and its supporting plate, while the 20-node solid element (SOLID186) that exhibits

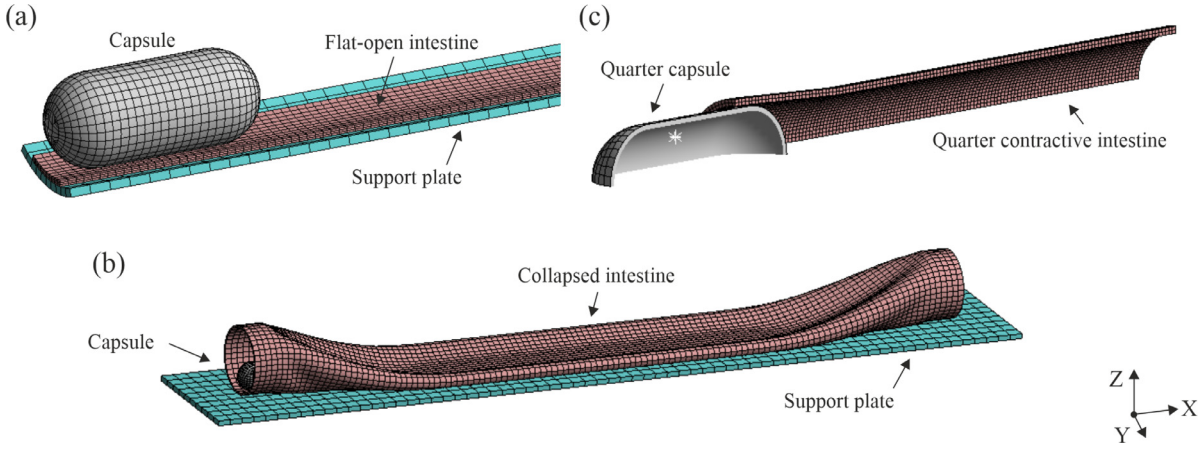

Fig. 4. (Colour online) FE models of (a) Case 1: cut-open intestine, (b) Case 2: collapsed intestine and (c) Case 3: contractive intestine.

quadratic displacement behaviour, having three degrees of freedom at each node, was used to simulate the viscoelastic intestine. The constraint and the loading conditions were applied to the capsule, the intestine and the supporting plate in three steps. In the first step, the lower surface of the plate was fixed to support the intestine and the moving capsule. Secondly, the standard earth gravity $9.81\ \mathrm{m/s^2}$ was applied to the entire model. Finally, the capsule moved for 150 mm along the intestine under various constant speeds between 0.5 and 10 mm/s.

In Case 2, the capsule moves inside a collapsed intestine whose upper wall drops down naturally due to the gravity. The FE model for this case is shown in Fig. 4(b), where the small intestine has an inner radius of 13 mm and a length of 250 mm laid on a supporting plate, and the capsule was positioned at the lifted entry of the intestine. The contact attribute between the intestine and its supporting plate was set as rough, indicating that there was no slip between the small intestine and the plate, but they can be separated and fitted freely. In addition, the bottom surface of the supporting plate was fully constrained, and the inlet and the outlet of the small intestine were also lifted and fixed. Loading step for Case 2 was considered in two steps. In the first step, the gravity acting on the entire model was evenly applied for a few seconds. Then, the capsule moved 250 mm along the intestine under various constant speeds between 0.5 and 10 mm/s.

Based on the above assumptions, due to the symmetry of the model, only a quarter of Case 3 was considered in the FE simulation as presented in Fig. 4(c). The intestine model in Case 3 consists of a trumpet-shaped inlet followed by a straight section with an inner diameter smaller than the outer diameter of the capsule. The total length of the small intestine was configured as 70 mm, and the inner diameter of the intestine was set as 10 mm, while the outer diameter of the capsule was 11 mm. The material properties of the capsule and the small intestine are listed in Table 1. Here, it is worth noting that Young's modulus of the small intestine E_f was measured from our previous relaxation tests [20]. Considering that the tensile modulus of the capsule is much larger than the small intestine, the capsule was set as a rigid body in Case 3 for reducing the computational cost. The contact pair between the capsule and the small intestine was set as frictional with the friction coefficient $\mu = 0.2293$ identified in our experiments [22]. For obtaining a better convergence, the capsule-intestine contact algorithm was configured as Pure Penalty, and the normal contact stiffness factor was set as 1. In addition, the same element type as Case 1 was used for Case 3 meshing, and a double-layer meshing was developed for the small intestine. In order to be consistent with our experimental setup, the boundary conditions at both ends of the intestine are different. At the inlet of the intestine, the movement of the intestine was restricted along the axial direction of the intestine, while it was set free at the outlet, so the intestine can be elongated when the capsule moves inside. This configuration can avoid the occurrences of stress singularity and computational error due to the distortion of the small intestine. Finally, the FE results for various constant speeds of the capsule between 0.5 and 10 mm/s were obtained from the middle section of the intestine that was far away from both ends according to the Saint Venants Principle.

The inner diameter of the curved intestine in Case 4 was set as 10 mm, and the dashed circle line in Fig. 5(a) denotes the central axis of the intestine. In our FE studies, different radii R of the circle were considered to test the passage of the capsule at different bending angles of the intestine. As the computation of the three-dimensional model of Case 4 is very time-consuming, a plane-symmetric model was developed to reduce the computational cost. To load the capsule's displacement along the intestinal tract, a frictionless rotation-slide mechanism shown in Fig. 5(b) was designed, consisting of a fixed bushing, a L-shaped revolving shaft and a slider that can force the capsule to follow a pre-defined trajectory. The axis of the fixed bushing coincided with the centre of the dashed circle as well as the axis of the L-shaped revolving shaft, and the centre of the capsule was fixed with the slider. When the capsule moves in the curved intestine, the force exerted on the capsule from the inner and the outer sidewalls of the intestine may not be equal. In order to achieve a mechanical equilibrium in FE analysis, the capsule will conduct a radial movement relative to the curvature. Therefore, the slider attached to the capsule was set to move freely along the sliding chute of the L-shaped revolving shaft. The material properties of the capsule and the small intestine are the same as the ones used in Case 3. In terms of intestinal boundary conditions as shown in Fig. 5(c), the inlet of the curved intestine and the red curve along the inner surface of the small intestine were restricted. These conditions imitate the situation that the small intestine is restrained by the mesentery in the abdominal cavity as illustrated in Fig. 5(d). However, the presence of mesentery depends on the age group of the patient. For example, elder patient might not have such an influence from the mesentery. So, in the following FE studies, both the intestines with and without mesentery were considered.

2.2.1. Contact setting and mesh convergence tests

To obtain more accurate results, contact setting and mesh convergence tests were carried out. The contact pressures and the resistance forces obtained from three various contact algorithms, the Pure Penalty, the Augmented Lagrange and the Normal Lagrange, were compared. The contact stiffness in Pure Penalty was altered from 0.01 to 5. As the normal stiffness in the Pure Penalty algorithm was reduced, both the contact pressure and the resistance force dropped down. By contrasting with all the results under the Normal Lagrange, the errors for the contact stiffness that are greater than or equal to 0.1 are all within ±5%. After compromising the calculating accuracy and the computational cost, the Pure Penalty with a normal contact stiffness of 1 was used as the subsequent capsule-intestine contact setting. Additionally, mesh convergence tests in all the cases were conducted by modifying intestine's mesh size. All capsule's mesh sizes were fixed at 1 mm, since the capsules were set as rigid bodies, and its mesh size will not affect convergence results. Table 2 provides the example of the mesh convergence tests for Case 3 with the consideration of a mesentery-like boundary, and its convergence results are presented in Fig. 6. It can be seen from the figure that the FE results (from Mesh 4 to 9) become stable when the element quantity of the model is more than 10,000. For the best performance of the FE model, the mesh size of the small intestine was selected as 0.5 mm, and the two mesh layers for the small intestine is sufficient for analysing the capsule-intestine contact at this stage.

3. Experimental apparatus

3.1. Experimental setup for speed-dependent analysis

The contact pressure between the capsule and the synthetic small intestine was investigated experimentally, and its experimental setup is shown in Fig. 7(a). A DC motor was used to pull and push the capsule linearly in the intestine at various constant speeds via a threaded shaft. Two pairs of RS PRO Foil strain gauges, forming a full Wheatstone bridge, were attached to the external surface of the capsule. The nominal gauge factor is 2.00, and it is suitable for measurement of both static and dynamic strains. The pressure on the capsule was calibrated by adjusting the depth of the capsule with the strain gauges within a cylinder filled with water. Their signals were amplified and then collected by a National Instrument data acquisition (DAQ) card via a graphic user interface (GUI) in LabVIEW. For a detailed introduction of the experimental setup and identified parameters, readers can refer to [20].

3.2. Experimental setup for vibro-impact motion recording

To explore the influence of the vibro-impact motion of the capsule on capsule-intestine contact pressure, the progression trajectory of the capsule along the small intestine needs to be recorded from the experiment, and then used for FE simulation. By using the experimental rig presented in Fig. 7(b), capsule's trajectory was recorded via a video camera. In the experiment, the vibro-impact motion of the capsule was generated by using an inner magnet excited by an external magnetic field.

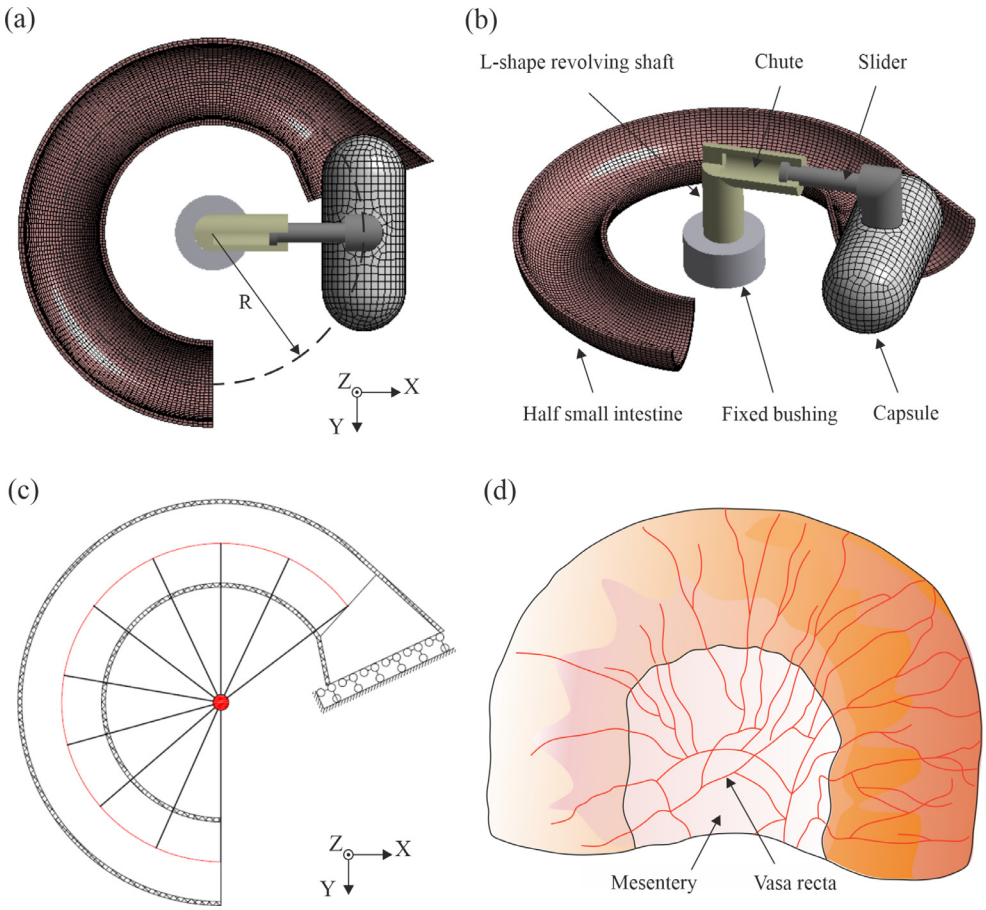

Fig. 5. (Colour online) (a) FE model of Case 4: curved intestine. The dashed circle line represents the central axis of the small intestine, and the curvature is represented by the radius R pointing to the dashed line. (b) The rotation-slide mechanism used in the Case 4 FE model to make sure the capsule follow a pre-defined trajectory and achieve a mechanical equilibrium coming from the inner and the outer sidewalls of the intestine. (c) Constraint setting of the curved intestine with mesentery. (d) Schematic diagram of the curved intestine with mesentery.

Table 2
Mesh convergence tests of Case 3 model with a mesentery-like boundary.

Test Method	Intestine Mesh Size (mm)	Capsule Mesh Size (mm)	Total Elements	Intestine Mesh Layers	Computational Time (mins)
Mesh 1	4	1	609	1	6
Mesh 2	2	1	903	1	7
Mesh 3	1	1	1,947	1	21
Mesh 4	0.5	1	11,583	2	172
Mesh 5	0.4	1	17,655	2	328
Mesh 6	0.35	1	33,033	3	453
Mesh 7	0.32	1	39,855	3	671
Mesh 8	0.28	1	51,039	3	994
Mesh 9	0.25	1	64,947	3	1,367

The magnetic field was generated by the coil driven by a square-wave excitation signal from a signal generator. The capsule was placed on a cut-open synthetic small intestine supported by a halved plastic tube, ensuring that the axis of the capsule coincides with the axis of the coil. The displacement of the capsule was recorded by a video camera located directly above the capsule, and the time series of the displacement were extracted by using an open source software. Again, for a detailed study of the experimental rig and procedure, readers can refer to [22].

4. Influence of capsule's speed

This section presents the speed-dependent analysis for Cases 1-4 with experimental comparison. Fig. 8 presents the time histories of the contact pressures for all the cases under a constant speed of the capsule at 0.5 mm/s. As can be seen from the figure, since the capsule entered the intestine from its trumpet-shaped inlet, the contact pressures for Cases 2-4 increased gradually. It is worth noting that the contact pressures in the grey areas of the figure were used for speed-dependent analysis.

The speed-dependent results for Case 1 are presented in Fig. 9(a), where the capsule moving at various constant speeds between 0.5 and 10 mm/s was tested. As can be seen from the figure, the average contact pressure was not affected obviously by the capsule's speed, but the maximum contact pressure increases as the capsule's speed increases. In general, the resistance force is getting smaller when the capsule's speed is increased except the measurement at the capsule's speeds of 1 and 2 mm/s. This may be due to the fact that the contact surface between the capsule and the intestine changes based on the capsule's speed. However, such a variation in resistance force (about 0.12 mN) is very small compared to the lowest measurement at 1 mm/s (about 7.71 mN). Experimental results for Case 1 are presented in Fig. 9(a) by using grey triangles with the grey line indicating its average. Comparing the FE and the experimental results, it can be seen that the averaged experi-

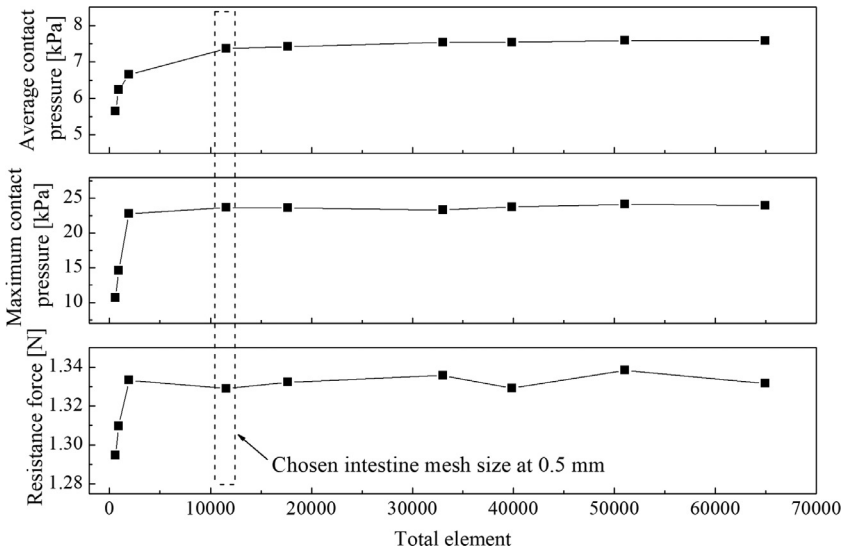

Fig. 6. Mesh convergence tests of Case 3 model with a mesentery-like boundary. Mesh 4 denoted by the dashed line with the intestine element size at 0.5 mm was chosen for further analysis.

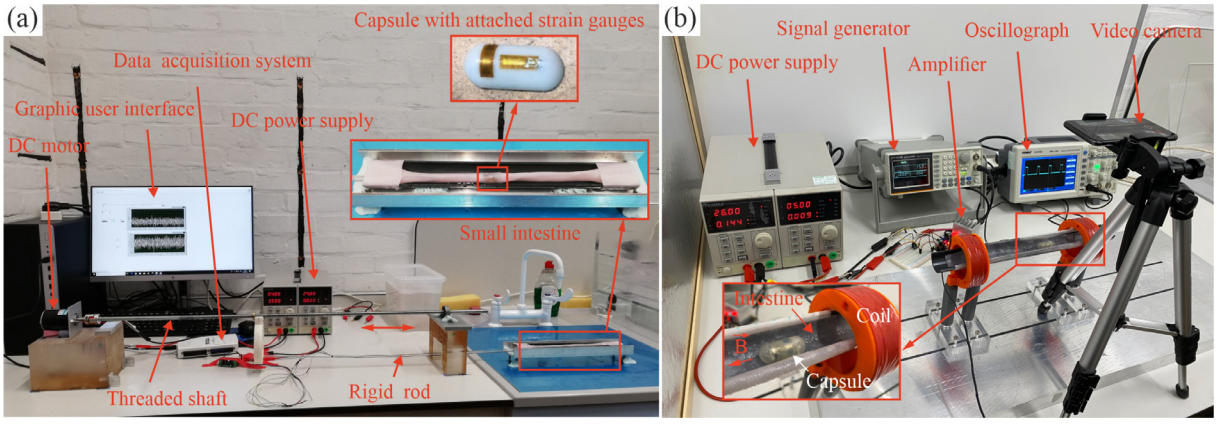

Fig. 7. (Colour online) Photographs of the experimental setups for (a) speed-dependent analysis and (b) vibro-impact motion recording. In speed-dependent analysis, a DC motor was used to drive the capsule inside the intestine at a constant moving speed, and the contact pressure was measured by two pairs of strain gauges attached on the capsule's outer surface, and the measurement signals were amplified and collected by a National Instrument data acquisition card via a graphic user interface in LabVIEW. In the vibro-impact experiment setup, a T-shaped magnet inside the capsule prototype was excited through an on-off electromagnetic field ***B*** and the helical spring to generate forward and backward impact motion, leading to the locomotion of the prototype. The on-off external excitation was produced and then amplified by a signal generator and a power amplifier. A video camera on the top of experiment rig was used to record the motion of the capsule, and then the displacement of the capsule was extracted by an open source software.

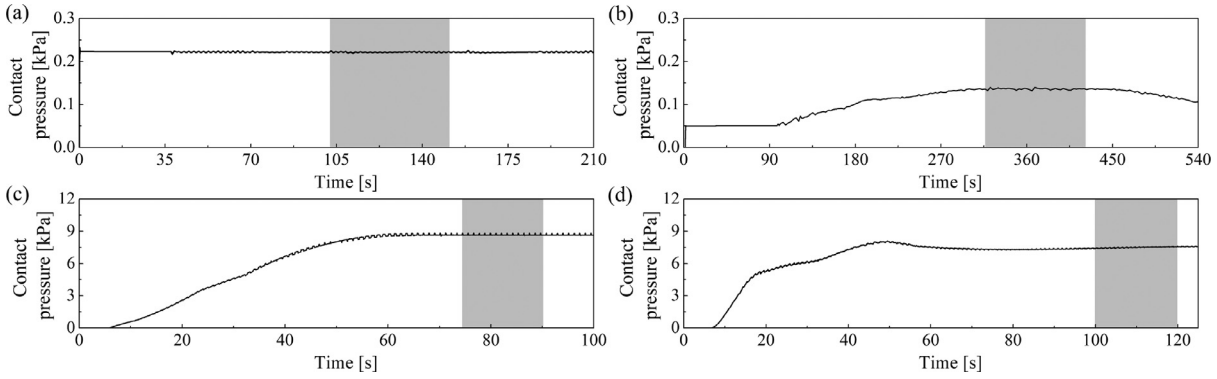

Fig. 8. Time histories of the contact pressures of the capsule in (a) Case 1, (b) Case 2, (c) Case 3 and (d) Case 4 moving at 0.5 mm/s. Grey areas indicate the contact pressures that were used for speed-dependent analysis.

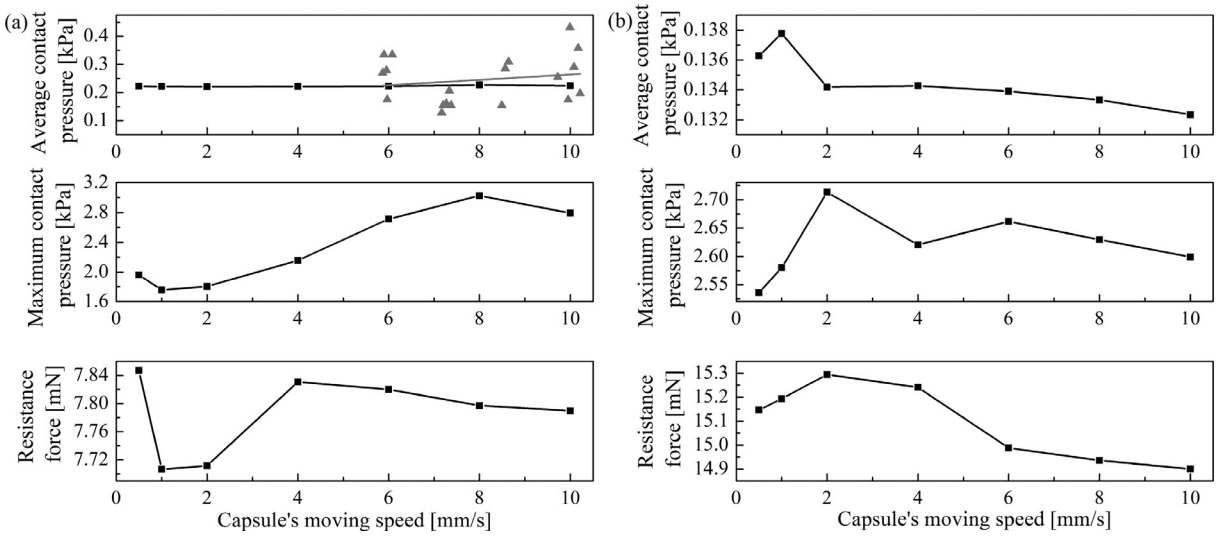

Fig. 9. FE speed-dependent results of (a) Case 1 and (b) Case 2. Grey triangles denote the experimental results, and the grey line indicates the average of the experimental results.

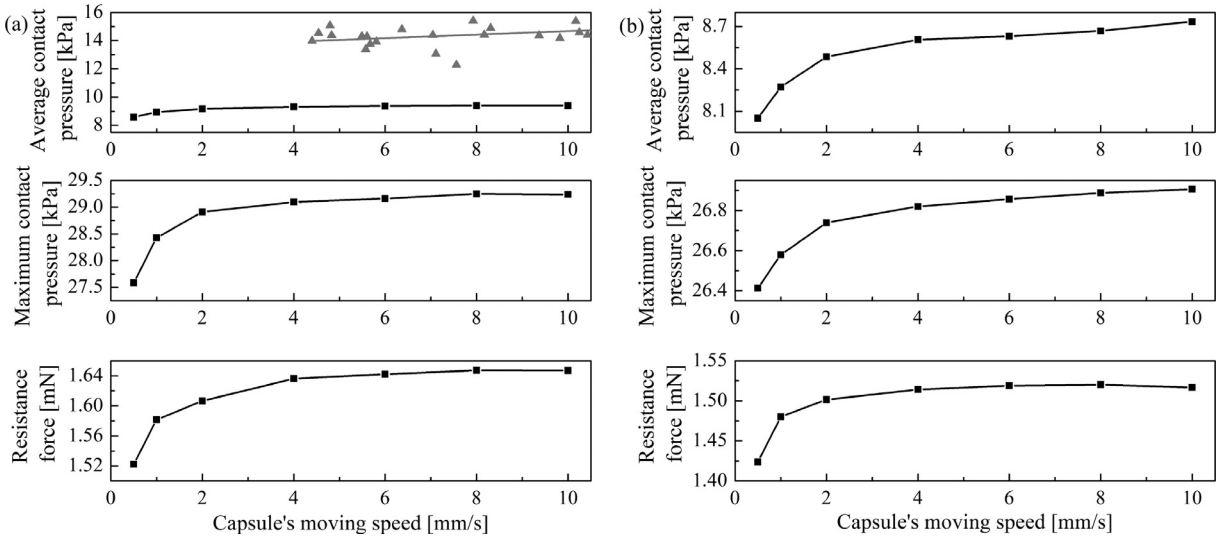

Fig. 10. FE speed-dependent results of (a) Case 3 and (b) Case 4. Grey triangles denote the experimental results, and the grey line indicates the average of the experimental results.

mental results are close to the FE simulations between 6 and 10 mm/s. In addition, the resistance forces under different capsule's speeds have small variations around 7.8 mN, which is also consistent with the experimental measurement in [31].

The speed-dependent results for Case 2 are shown in Fig. 9(b). As can be seen from the figure, as the capsule's speed increases in the collapsed intestine, the average contact pressure and the resistance force remain stable around 0.134 kPa and 15.2 mN, respectively. Compared to Case 1's results, the average contact pressure of Case 2 is lower than that of Case 1, and the resistance force of Case 2 is nearly twice of Case 1. This is because that when the upper wall of the intestine naturally falls over the capsule in Case 2, its contact area with the capsule is doubled comparing to Case 1. However, the maximum contact pressures for both cases are very close with some minor differences, which may be caused by the additional weight of the upper intestinal wall acting on the capsule.

Fig. 10 (a) presents the FE speed-dependent results for Case 3. It can be seen from the figure that the average contact pressure increases slightly from 8.58 to 9.40 kPa when the capsule's speed increases from 0.5 to 10 mm/s, fitting well with the trend of the experimental results denoted by grey triangles with the grey line indicating its average. However, the FE results are much lower than the averaged pressure measured via experiment (about 14.5 kPa). Such a difference was caused by the unloading of the gravity in Case 3's model. Also, when the external diameter of the capsule is larger than the internal diameter of the small intestine, intestinal hoop pressure will dominate the contact pressure between the capsule and the intestine, which is very sensitive to the experimental setup and could cause a significant difference in measurement. From a general observation of the FE results, it can be concluded that the contact pressure and the resistance force become less sensitive to the capsule's speed once it is more than 4 mm/s.

The speed-dependent results for Case 4 when the capsule moved through a curved intestine with a bending radius of 15 mm are shown in Fig. 10(b). As the capsule moved faster, it can be observed from the figure that the average contact pressure raised from 8.05 to 8.73 kPa, the maximum contact pressure increased from 26.41 to 26.91 kPa, and the resistance force went up from 1.42 to 1.52 N. Compared to Case 3, all

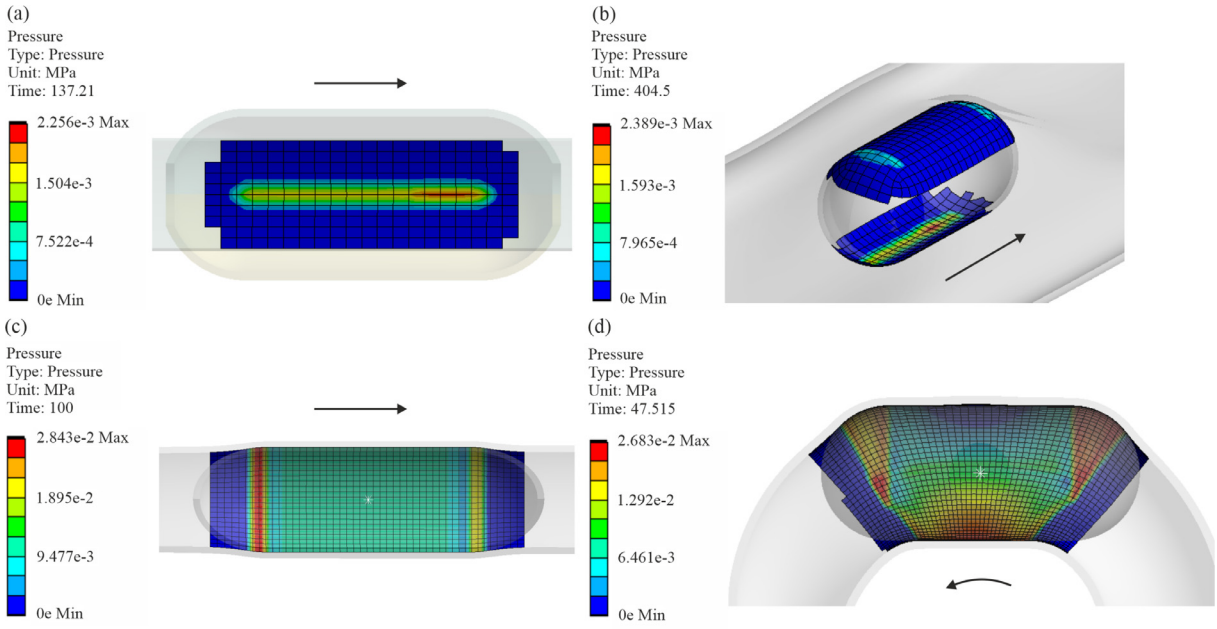

Fig. 11. (Colour online) Contact pressure distribution for (a) Case 1, (b) Case 2, (c) Case 3 and (d) Case 4. The bending radius of Case 4 is 15 mm, and the capsule's speed is 0.5 mm/s. The arrow indicates the moving direction of the capsule.

these values are slightly lower in Case 4. These differences were cased by the incomplete capsule-intestine contact in the curved intestine, while the straight intestine can provide a full contact with the capsule.

The contact pressure distribution of the FE simulation for each case is shown in Fig. 11. The rectangular blue area which is about 15 mm in width and 2.6 mm in height shown in Fig. 11(a) is the capsule-intestine contact area for Case 1. For Case 2 as shown in Fig. 11(b), both the upper and lower intestinal walls had contact with the capsule, and the contact pressure mainly distributed at the lower surface of the capsule. The maximum pressures for Case 1 and 2 located at the front of lower surface of the capsule along its moving direction, indicating that the capsule tilted down slightly when moving forward. For Case 3, Fig. 11(c) presents the distribution of the hoop pressure between the capsule and the contractive intestine. Higher pressure distributed at both ends of the cylindrical surface of the capsule. In particular, the contact pressure at the tail (left) of the capsule is much larger than that of the capsule's head (right), which was caused by the stress relaxation of the synthetic material of the small intestine. In detail, as the straight intestine behind the moving capsule was elongated due to the boundary constrains on the left entrance of the intestine, while the small intestine in the forward direction of the capsule was free, the capsule's tail experienced more pressure. In Fig. 11(d), the concentration of the contact pressure in the curved intestine was distributed at the capsule's head and tail regions, as well as the lower surface of the capsule. This was due to the fact that the upper intestinal wall was expanded, and the lower wall was compressed.

5. Influence of the mesentery

The influence of the bending radius of the intestine on capsule-intestine contact with and without the mesentery is presented in Fig. 12. As can be seen from Fig. 12(a), both the contact pressure and the resistance force changed dramatically with the variation of the curved radius. The maximum contact pressure increased from 23.80 to 36.36 kPa when the bending radius was decreased from 25 to 10 mm in the presence of the mesentery. As the bending radius increased from 25 mm to infinity (i.e. straight intestine), only small variations in the contact pressure and the resistance force can be observed. For the influence without the consideration of the mesentery shown in Fig. 12(b), the maximum contact pressure varied from 45.37 to 28.14 kPa as the bending radius increased from 10 to 400 mm. By comparing Figs. 12(a) and (b), it can reveal that the mesentery does affect the interactions between the capsule and the intestine, particularly when the bending radius of the curved intestine is small. It also can be observed that the contact pressure and the resistance force without the presence of the mesentery are much larger than the ones with the mesentery. However, as the bending radius of the curved intestine increases, the contact pressure and the resistance become stable which are close to the ones obtained from the straight intestine.

By taking the curved intestines with the bending radii at 20 and 200 mm as examples, the stress distributions of the intestines with and without the mesentery are presented in Fig. 13. As can be seen from Fig. 13(a) and (b), the mesentery kept the intestine at its original gesture when the capsule was passing through, but the intestine without the mesentery was straightened by the moving capsule. It also can be observed from Fig. 13(a) and (c) that, the stress on the intestine mainly distributed around the capsule. Higher stress can be found from the lower intestinal wall when the bending radius is small. As the bending radius increases, the stress concentration moves to the upper intestinal wall around the head of the capsule. For the curved intestine without the mesentery shown in Fig. 13(b) and (d), the stress concentration located at the upper wall around the tail of the capsule, and the intestine behind the capsule was stretched significantly. Therefore, the mesentery and the non-mesentery boundary conditions on the small intestine can lead to completely different results for capsule-intestine interaction. However, such a difference is not so significant when the bending radius of the curved intestine is large.

6. Influence of capsule's shape

To understand the influence of the capsule's shape on the capsule-intestine interaction, various shapes of the capsule by changing the lengths of its both ends were studied in Case 3. The geometry of the capsule is presented in Fig. 14, where the capsule consists of a cylindrical body with 15 mm in length, 11 mm in diameter, 0.5 mm in thickness and two symmetric semi-elliptical ends with a length of L_a.

The FE results of Case 3 as functions of the semi-elliptical end's length are presented in Fig. 15(a) with the capsule's speed at 10 mm/s.

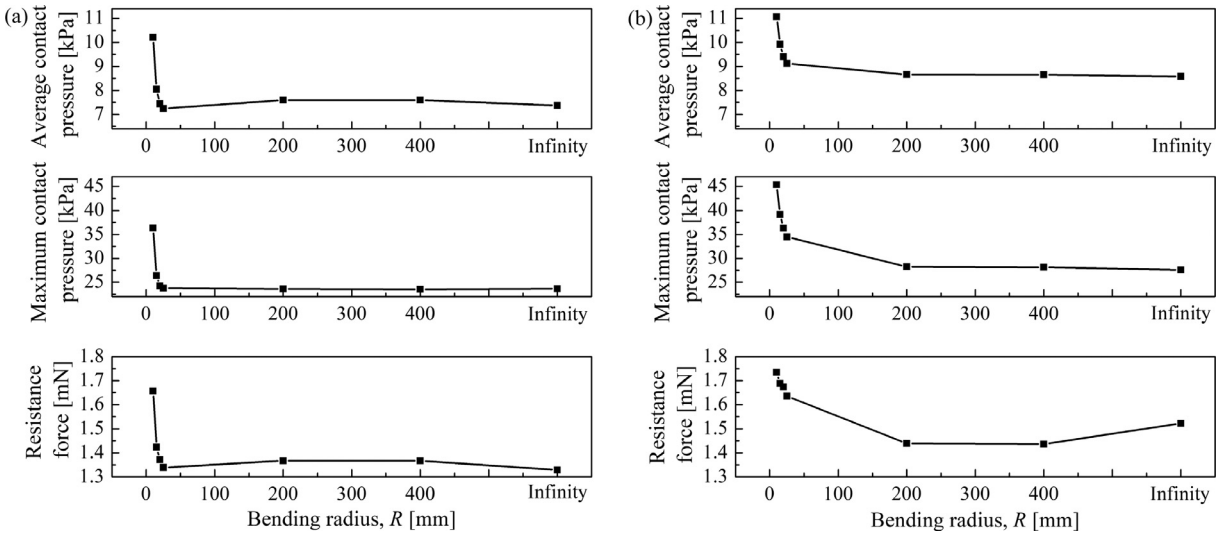

Fig. 12. FE results of the curved intestine (a) with and (b) without the mesentery computed for different bending radii with the capsule's speed at 0.5 mm/s. Infinite radius refers to the straight intestine in Case 3.

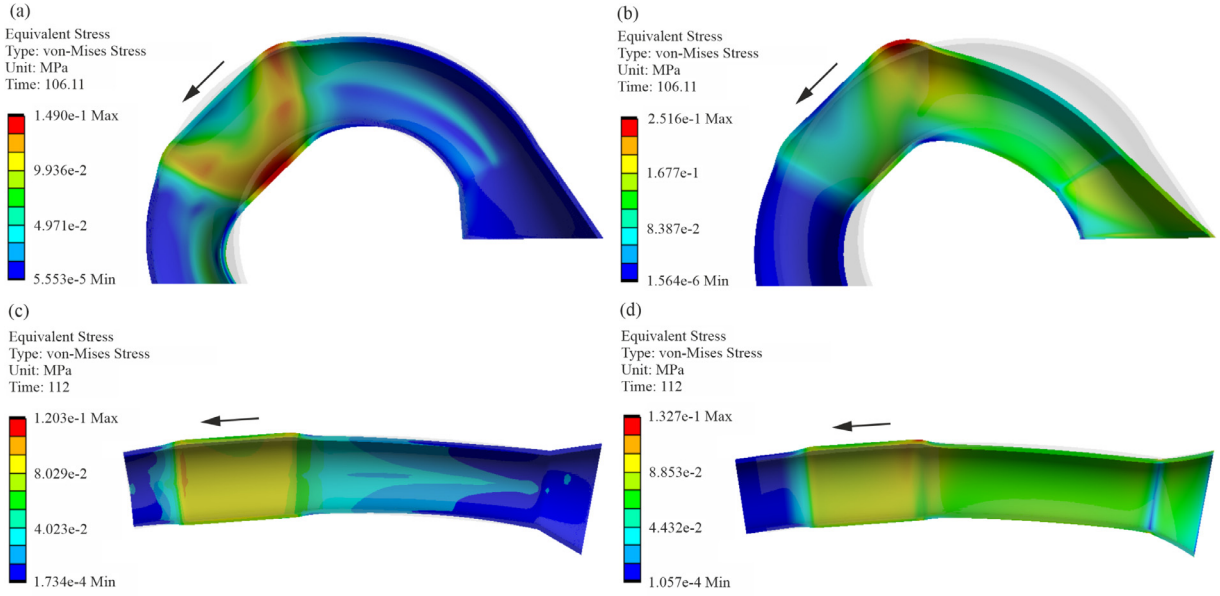

Fig. 13. (Colour online) Stress distribution of the curved intestines with the bending radii at (a,b) 20 mm and (c,d) 200 mm, where (a,c) and (b,d) are the curved intestines with and without the mesentery, respectively. All the capsules moved at a constant speed of 0.5 mm/s. The shadow area indicates the original gesture of the intestine. The arrow denotes the instantaneous movement direction of the capsule.

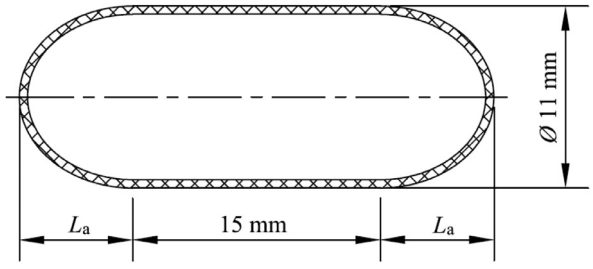

Fig. 14. Dimension of the capsule prototype, where the thickness of the capsule is 0.5 mm.

As this length increased, both the average contact and the maximum contact pressures decreased, but the resistance force increased from 1.45 to 1.63 N. Furthermore, the maximum contact pressure was more sensitive to the variation of the capsule's shape decreasing from 53.28 to 16.76 kPa. On one hand, a moderate increase of the intestinal resistance may help the capsule's control and improve the efficiency of its movement. On the other hand, larger contact pressure may induce pain to the patients and even damage the intestinal tissue. In order to compromise these facts, the optimum length of the semi-elliptical end is suggested to be 5.5 mm.

The qualitative evaluation of the trauma level was carried out by Li et al. [48], which performed a reciprocating friction test by simulating a surgeon's finger sliding on the surface of a rabbit's small intestine for 1, 3 and 5 minutes. This corresponds to the real scenario that the self-propelled capsule is stuck in the small intestine for some time, and the vibro-impact motion of the capsule may cause this reciprocating sliding at one position of the intestinal wall. By comparing the maximum contact pressures with the pressure-trauma relationship shown in Fig. 15(b), it can be noted that even with the length of 8.25 mm (the lowest maximum contact pressure), the capsule may cause the hyperemia of the intestinal wall (tissue trauma level is greater than level 1) if the vibro-

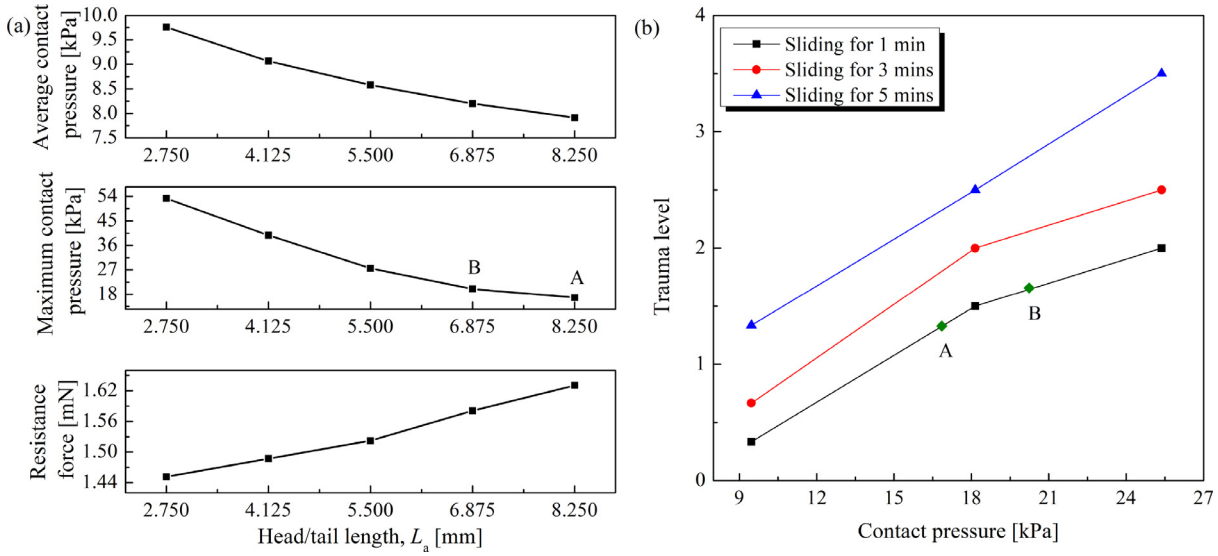

Fig. 15. (a) FE results of Case 3 as functions of the semi-elliptical end's length. (b) Qualitative evaluation of the intestinal trauma induced by capsule-intestine interaction. All the capsules moved at a constant speed of 10 mm/s. Points A and B correspond to the maximum contact pressures A and B in (a), respectively. The trauma levels 1 to 4 correspond to the hyperemia, the hemorrhage, the degeneration, and the necrosis (adapted from [48]), respectively.

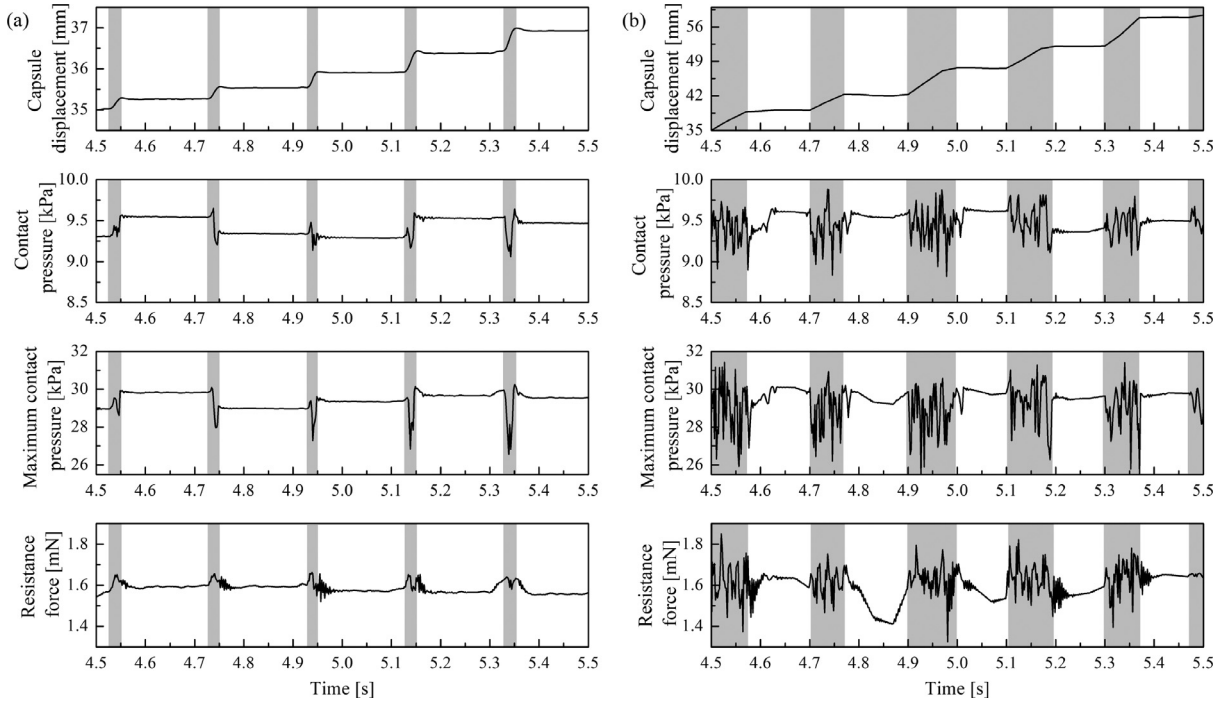

Fig. 16. FE results computed by using the capsule displacement measured from experiments under (a) the excitation frequency 5 Hz and the duty cycle 20% and (b) the excitation frequency 5 Hz and the duty cycle 50%. Grey and blank areas denote the slip and stick motions of the capsule, respectively.

impact motion lasts for 1 minute. Compared with Figs. 9 and 10, the capsule moving on the cut-open and the collapsed intestines are safe, while the capsule moving in the contractive and the curved intestines may cause trauma. Therefore, when the capsule is stuck in the intestine, a long-time reciprocating sliding motion may scratch intestinal mucosa and cause muscular bleeding. To avoid this injury, temporarily suspension of vibro-impact motion of the capsule is recommended when it is stuck in the intestine. Wang et al. [50] have shown that the use of appropriate lubricant (e.g. calf serum or hyaluronic acid) can relieve the traumas and reduce the friction at the probe-intestine mucosa interface during the insertion process of enteroscopy. However, this may reduce the motion efficiency of the capsule as lubricant will reduce the friction at the capsule-intestine interface, so locomotion control of the capsule may become more challenging.

7. Influence of the vibro-impact motion

In this section, the influence of the vibro-impact motion recorded from our experiment on the capsule-intestine interaction was investigated. Direct measurement of the contact pressure will require the attachment of strain gauges on the capsule, which may affect the dynamics of the system. Also, such a measurement may not give a timely logging in response to the vibro-impact motion between 5 and 40 Hz due to the existence of response delay in strain gauges. So, using the recorded

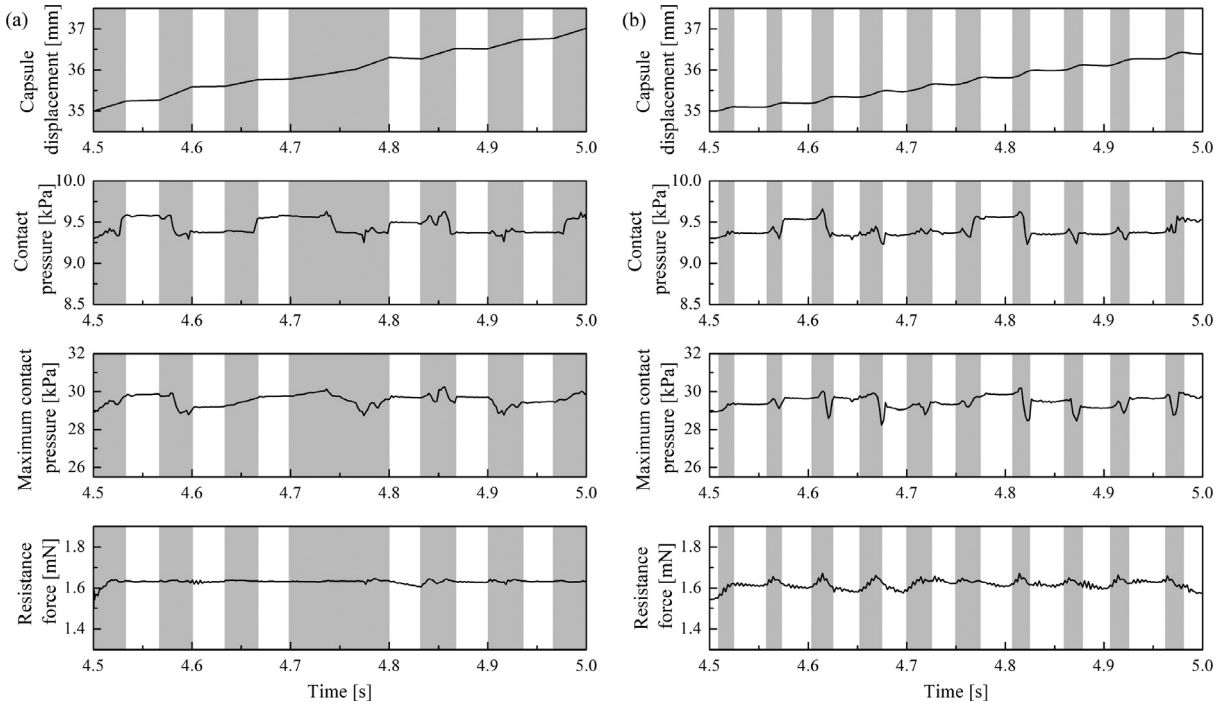

Fig. 17. FE results computed by using the capsule displacement measured from experiments under (a) the excitation frequency 15 Hz and the duty cycle 50% and (b) the excitation frequency 20 Hz and the duty cycle 20%. Grey and blank areas denote the slip and stick motions of the capsule, respectively.

displacement of the capsule as an input of the FE model is a viable approach to learn the capsule-intestine interaction under the vibro-impact motion.

Figs. 16 and 17 show the time histories of the recorded vibro-impact motion of the capsule under different control parameters and the corresponding contact pressures and resistance forces computed using the FE model of Case 3. It can be seen from the figure that stick-slip motions of the capsule were recorded, where grey and blank areas indicate the slip and stick motions of the capsule, respectively. It is obvious that the contact pressures and the resistance forces remain relatively stable in the sticking phase, while fluctuated in the slipping phase. By comparing Fig. 16(a) with (b), the higher the duty cycle of the excitation was, the longer the slipping phase was, and this led to a longer duration of fluctuation in the capsule-intestine interaction. Here, the duty cycle is the fraction of one period in which the on-off excitation is active. For Fig. 17(a) and (b), when the frequency of the excitation was increased, fluctuations are not that significant compared to Fig. 16(b). Therefore, the stick-slip motion of the capsule may cause more obvious fluctuations on the contact pressure so as the resistance force compared to the scenarios of the capsule with a constant moving speed. However, the overall fluctuations are minor compared to the original pressure levels at the sticking phase.

8. Concluding remarks

Analysis of a self-propelled capsule robot moving in the small intestine was conducted in this paper via FE modelling and experiment. Based on the anatomy of the small intestine, four typical capsule-intestine contact cases were considered. In addition to our previous work [20,31], we firstly considered the capsule moving in a curved intestine, the intestines with and without the mesentery, the capsule's geometry with respect to the trauma level, and the effect of the capsule's vibro-impact motion on the intestine. According to the extensive numerical and experimental studies in this paper, the general conclusion is that the vibro-impact motion of the capsule may potentially induce trauma on the intestinal wall if the vibro-impact capsule is stuck in the intestine.

For the four contact cases, the contact pressure and the resistance force between the capsule and the intestine were studied by varying capsule's speeds. When the capsule moves on the cut-open and in the collapsed intestines, the contact pressure and the resistance force are less dependent on the capsule's moving speed. For the collapsed intestine, the resistance force on the capsule is about twice of the one for the cut-open intestine. When the capsule moves in the contractive and the curved intestines, faster speed of the capsule could lead to greater contact pressure and resistance force. In addition, experimental results adopted from Guo et al. [20] were used to confirm the FE modelling in this work.

For the capsule moving in the curved intestine, different curvatures of the intestine were studied. It was found that the contact pressure and the resistance force could increase dramatically for the bending radius between 10 and 25 mm, while they are close to those of a straight intestine when the bending radius is greater than 200 mm. In addition, the contact pressure and the resistance force for the intestine without the mesentery are greater than the ones with the mesentery because of the restriction of deformation on the intestine.

To optimise the geometry of the capsule, we focused on the influence of length of the capsule's both ends and the potential trauma level that it may cause. It was found that the longer of the capsule's end is, the greater the resistance force and the lower the contact pressure are. In order to compromise this, a rounded capsule's end (i.e. the radius of the capsule's cylindrical body equals to the length of the capsule's end) is recommended. To evaluate the trauma level adopted from [48], when the capsule is stuck in the intestine, the long-time reciprocating sliding motion of the capsule may scratch the intestinal mucosa and cause muscular bleeding. Therefore, to avoid such an injury, temporal suspension of capsule's vibro-impact motion is recommended when it is stuck in the intestine.

When the vibro-impact motion of the capsule in the small intestine was considered, fluctuations can be observed from the capsule-intestine interaction which mainly occurred at the slipping phase of the capsule. However, the overall fluctuations are minor compared to the original pressure levels at the sticking phase. To summarise the findings of

the present work, the contact pressure is very sensitive to the dynamic movement patterns of the small intestine, i.e. peristalsis and segmentation, and the complex anatomy of the intestine, such as mesenteric and non-mesenteric intestines and intestinal spatial posture. A proper design of the capsule's head and tail length can reduce the resistance force and the trauma level significantly, so such a parameter can be used as one of the design variables for tissue trauma exploration. Finally, the fluctuations in the contact pressure induced by the capsule's vibro-impact motion are minor. In a nutshell, it is essential to provide guidance for the control design of the self-propelled vibro-impact capsule robot in terms of the complexity of the intestine, the dimension of the capsule and the means of propulsion, to be clinically acceptable.

Considering future works, the complete capsule model including the onboard vibro-impact mechanism will be studied for these four contact cases through FE simulation. The model of the small intestine should be depicted further in detail, including the intestinal haustra, peristalsis and segmentation, and bowel lesion. The locomotion controls of the capsule robot in an ascending or a descending segment and in a curved intestine are also vital for an efficient endoscopic examination. These future works will be presented in a separate publication in due course.

Compliance with ethical standards.

Conflict of interest. The authors declare that they have no conflict of interest concerning the publication of this manuscript.

Data accessibility. The numerical and experimental data sets generated and analysed during the current study are available from the corresponding author on reasonable request.

Declaration of competing interest

The authors declare that they have no known competing financial interests or personal relationships that could have appeared to influence the work reported in this paper.

CRediT authorship contribution statement

Jiyuan Tian: Methodology, Software, Validation, Formal analysis, Investigation, Writing – original draft, Visualization. **Yang Liu:** Conceptualization, Methodology, Writing – review & editing, Visualization, Supervision, Project administration, Funding acquisition. **Junning Chen:** Conceptualization, Methodology, Writing – review & editing, Supervision. **Bingyong Guo:** Methodology, Writing – review & editing. **Shyam Prasad:** Conceptualization, Methodology, Supervision.

Acknowledgement

This work has been supported by EPSRC under Grant No. EP/R043698/1. Mr Jiyuan Tian would like to acknowledge the financial support from China Scholarship Council for his CSC-Exeter PhD scholarship (award no. 201908060172). The authors would like to acknowledge Miss Jiajia Zhang for providing her experimental data from the vibro-impact capsule experiment.

Appendix A

The equations of motion of the vibro-impact capsule system [22] shown in Fig. 2(a) can be written as

$$\begin{cases} m_1\ddot{x}_1 = F_p - F_i, \\ m_2\ddot{x}_2 = F_f + F_i, \end{cases}$$

where x_1 and x_2 are the displacements of the magnet and the capsule, respectively. F_i is the interaction force between the capsule and the magnet given as

$$F_i = \begin{cases} k_1(x_1 - x_2) + c(v_1 - v_2) + F_2, & x_1 - x_2 \leqslant -G_2, \\ k_1(x_1 - x_2) + c(v_1 - v_2), & -G_2 \leqslant x_1 - x_2 \leqslant G_1, \\ k_1(x_1 - x_2) + c(v_1 - v_2) + F_1, & x_1 - x_2 \geqslant G_1, \end{cases}$$

where v_1 and v_2 are the velocities of the magnet and the capsule, respectively. $F_1 = k_3(x_1 - x_2 - G_1)$ and $F_2 = k_2(x_1 - x_2 + G_2)$ represent the impact forces by the secondary and the primary constraints, respectively. F_p is the external forcing on the magnet implemented by a square wave signal expressed as

$$F_p(t) = \begin{cases} P_d, & t \in [nT, nT + DT], \\ 0, & t \in (nT + DT, nT + T), \end{cases}$$

where n is the period number. P_d, T and $D \in (0, 1)$ are the amplitude, period and duty cycle ratio of the signal, respectively. Here, the intestinal resistance between the capsule and the small intestine, F_f, can be written as

$$\begin{cases} F_f \in [-P_f, P_f], & v_2 = 0, \\ F_f = -sign(v_2)P_f, & v_2 \neq 0, \end{cases}$$

where $P_f = \mu(m_1 + m_2)g$ is the static friction of the capsule, μ is the friction coefficient and g is the gravitational acceleration.

References

[1] Mc Caffrey C, Chevalerias O, O'Mathuna C, Twomey K. Swallowable-capsule technology. IEEE Pervasive Comput 2008;7(1):23–9.
[2] Bouchard S, Ibrahim M, Van Gossum A. Video capsule endoscopy: perspectives of a revolutionary technique. World J Gastroenterol 2014;20(46):17330–44.
[3] Le Mouel J-P, Fumery M, Hakim S, Yzet C, Dervaux A, Dray X, Nguyen-Khac E. Type 2 refractory celiac disease on third-generation capsule endoscopy and enteroscopy: typical appearance of ulcerative jejunitis. Endoscopy 2020;52(06):E195–7.
[4] Adler SN, Lama YG, Royo VM, Ferrer CS, Schwartz A, Shitrit AB-G. Comparison of small-bowel colon capsule endoscopy system to conventional colonoscopy for the evaluation of ulcerative colitis activity. Endoscopy Int Open 2019;7(10):E1253–61.
[5] PillcamSB 3 system, medtronic: capsule endoscopy products. https://www.medtronic.com/covidien/en-us/products/capsule-endoscopy/pillcam-sb-3-system.htmlAccessed 16 September 2020.
[6] Mirocam capsule endoscope system. https://www.intromedic.com:549/eng/main/. Accessed 16 September 2020.
[7] Omom capsule endoscopy. http://english.jinshangroup.com/capsuleendoscopy.html. Accessed 16 September 2020.
[8] Singeap A-M, Stanciu C, Trifan A. Capsule endoscopy: the road ahead. World J Gastroenterol 2016;22(1):369.
[9] Koulaouzidis A, Iakovidis DK, Karargyris A, Rondonotti E. Wireless endoscopy in 2020: will it still be a capsule? World J Gastroenterol 2015;21(17):5119.
[10] Capsule endoscopy, saint luke's health system. https://www.saintlukeskc.org/health-library/capsule-endoscopy. Accessed 10 October 2020.
[11] Valdastri P, Simi M, Webster III RJ. Advanced technologies for gastrointestinal endoscopy. Ann Rev Biomed Eng 2012;14:397–429.
[12] Hall JE. Guyton and hall textbook of medical physiology. 1st. Jordan: Elsevier; 2016.
[13] Byrnes KG, Walsh D, Dockery P, McDermott K, Coffey JC. anatomy of the mesentery: current understanding and mechanisms of attachment. Seminars Cell Dev Biol 2019;92:12–17.
[14] Smith M, Morton D. The digestive system, basic science and clinical conditions. 2nd. Toronto: Elsevier; 2010.
[15] Hinck L, Näthke I. Changes in cell and tissue organization in cancer of the breast and colon. Curr Opinion Cell Biol 2014;26:87–95.
[16] Ciarletta P, Dario P, Tendick F, Micera S. Hyperelastic model of anisotropic fiber reinforcements within intestinal walls for applications in medical robotics. Int J Robotic Res 2009;28(10):1279–88.
[17] Zhang C, Liu H, Li H. Modeling of frictional resistance of a capsule robot moving in the intestine at a constant velocity. Tribol Lett 2014;53(1):71–8.
[18] Kim J-S, Sung I-H, Kim Y-T, Kwon E-Y, Kim D-E, Jang YH. Experimental investigation of frictional and viscoelastic properties of intestine for microendoscope application. Tribol Lett 2006;22(2):143–9.
[19] Zhou H, Alici G, Than TD, Li W. Modeling and experimental characterization of propulsion of a spiral-type microrobot for medical use in gastrointestinal tract. IEEE Trans Biomed Eng 2012;60(6):1751–9.
[20] Guo B, Liu Y, Prasad S. Modelling of capsule–intestine contact for a self-propelled capsule robot via experimental and numerical investigation. Nonlinear Dyn 2019;98(4):3155–67.
[21] Zhang C, Liu H. Analytical friction model of the capsule robot in the small intestine. Tribol Lett 2016;64(3:39):1–11.
[22] Liu Y, Páez Chávez J, Zhang J, Tian J, Guo B, Prasad S. The vibro-impact capsule system in millimetre scale: numerical optimisation and experimental verification. Meccanica 2020;55(10):1885–902.
[23] Kim HM, Yang S, Kim J, Park S, Cho JH, Park JY, Kim TS, Yoon E-S, Song SY, Bang S. Active locomotion of a paddling-based capsule endoscope in an in vitro and in vivo experiment (with videos). Gastrointestinal Endoscopy 2010;72(2):381–7.
[24] Sun Z-J, Ye B, Qiu Y, Cheng X-G, Zhang H-H, Liu S. Preliminary study of a legged capsule robot actuated wirelessly by magnetic torque. IEEE Trans Magnetic 2014;50(8):1–6.
[25] Gao J, Yan G. Locomotion analysis of an inchworm-like capsule robot in the intestinal tract. IEEE Trans Biomed Eng 2015;63(2):300–10.

[26] Carta R, Tortora G, Thoné J, Lenaerts B, Valdastri P, Menciassi A, Dario P, Puers R. Wireless powering for a self-propelled and steerable endoscopic capsule for stomach inspection. Biosensor Bioelectron 2009;25(4):845–51.
[27] Liu Y, Wiercigroch M, Pavlovskaia E, Yu H. Modelling of a vibro-impact capsule system. Int J Mech Sci 2013;66:2–11.
[28] Sfakiotakis M, Pateromichelakis N, Tsakiris DP. Vibration-induced frictional reduction in miniature intracorporeal robots. IEEE Trans Robotic 2014;30(5):1210–1221.
[29] Chernous'ko FL. The optimum rectilinear motion of a two-mass system. J Appl Math Mech 2002;66(1):1–7.
[30] Liao M, Liu Y, Páez Chávez J, Chong AS, Wiercigroch M. Dynamics of vibro-impact drilling with linear and nonlinear rock models. Int J Mech Sci 2018;146:200–10.
[31] Guo B, Ley E, Tian J, Zhang J, Liu Y, Prasad S. Experimental and numerical studies of intestinal frictions for propulsive force optimisation of a vibro-impact capsule system. Nonlinear Dyn 2020;101(1):65–83.
[32] Yan Y, Liu Y, Jiang H, Peng Z, Crawford A, Williamson J, Thomson J, Kerins G, Yusupov A, Islam S. Optimization and experimental verification of the vibro-impact capsule system in fluid pipeline. Proc Inst Mech Eng Part C: J Mech Eng Sci 2019;233(3):880–94.
[33] Liu Y, Pavlovskaia E, Hendry D, Wiercigroch M. Vibro-impact responses of capsule system with various friction models. Int J Mech Sci 2013;72:39–54.
[34] Nguyen V-D, Duong T-H, Chu N-H, Ngo Q-H. The effect of inertial mass and excitation frequency on a duffing vibro-impact drifting system. Int J Mech Sci 2017;124:9–21.
[35] Duong T-H, Nguyen V-D, Nguyen H-C, Vu N-P, Ngo N-K, Nguyen V-T. A new design for bidirectional autogenous mobile systems with two-side drifting impact oscillator. Int J Mech Sci 2018;140:325–38.
[36] Yan Y, Liu Y, Manfredi L, Prasad S. Modelling of a vibro-impact self-propelled capsule in the small intestine. Nonlinear Dyn 2019;96(1):123–44.
[37] Guo B, Liu Y, Birler R, Prasad S. Self-propelled capsule endoscopy for small-bowel examination: proof-of-concept and model verification. Int J Mech Sci 2020;174:105506.
[38] Liu Y, Páez Chávez J, Guo B, Birler R. Bifurcation analysis of a vibro-impact experimental rig with two-sided constraint. Meccanica 2020:1–17.
[39] Baek N, Sung I, Kim DE. Frictional resistance characteristics of a capsule inside the intestine for microendoscope design. Proc Inst Mech Eng Part H: J Eng Med 2004;218(3):193–201.
[40] Kim J, Sung I, Kim Y, Kim DE, Jang YH. Analytical model development for the prediction of the frictional resistance of a capsule endoscope inside an intestine. Proc Inst Mech Eng Part H: J Eng Med 2007;221(8):837–45.
[41] Wang X, Meng MQ. An experimental study of resistant properties of the small intestine for an active capsule endoscope. Proc Inst Mech Engineers, Part H: Journal of Engineering in Medicine 2010;224(1):107–18.
[42] Zhang C, Liu H, Tan R, Li H. Modeling of velocity-dependent frictional resistance of a capsule robot inside an intestine. Tribol Lett 2012;47(2):295–301.
[43] Zhang H, Yan Y, Gu Z, Wang Y, Sun T. Friction enhancement between microscopically patterned polydimethylsiloxane and rabbit small intestinal tract based on different lubrication mechanisms. ACS Biomater Sci Eng 2016;2(6):900–7.
[44] Wang Z, Ye X, Zhou M. Frictional resistance model of capsule endoscope in the intestine. Tribol Lett 2013;51(3):409–18.
[45] Woo SH, Kim TW, Cho JH. Stopping mechanism for capsule endoscope using electrical stimulus. Med Biol Eng Comput 2010;48(1):97–102.
[46] Wang KD, Yan GZ. Research on measurement and modeling of the gastro intestine's frictional characteristics. Measur Sci Technol 2008;20(1). 015803 (6 pages)
[47] Lyle AB, Terry BS, Schoen JA, Rentschler ME. Preliminary friction force measurements on small bowel lumen when eliminating sled edge effects. Tribol Lett 2013;51(3):377–83.
[48] Li W, Shi L, Deng H, Zhou Z. Investigation on friction trauma of small intestine in vivo under reciprocal sliding conditions. Tribol Lett 2014;55(2):261–70.
[49] Syndaver labs: small intestine. http://syndaver.com/shop/syndaver. Accessed 4 November 2019.
[50] Wang J, Ma L, Li W, Zhou Z. Influence of different lubricating fluids on friction trauma of small intestine during enteroscopy. Tribology International 2018;126:29–38.